Complex InSAR radar image processing, GNSS, and TPS measurements to determine the Kaniv HPP dam deformations

Kornyliy Tretyak
Lviv Polytechnic National University: Nacional'nij universitet L'vivs'ka politehnika
Svitlana Nesterenko (NesterenkoS2208@gmail.com)
Lviv Polytechnic National University: Nacional'nij universitet L'vivs'ka politehnika
https://orcid.org/0000-0002-2288-3524
Yuriy Bisovetskyi
PGSC "Ukrhydroenergo"

Research Article

Keywords: deformation monitoring, vertical displacements, GNSS measurements, TPS measurements, differential interferometry (DInSAR), dam

Posted Date: December 4th, 2023

DOI: https://doi.org/10.21203/rs.3.rs-3426456/v1

Complex InSAR radar image processing, GNSS, and TPS measurements to determine the Kaniv HPP dam deformations

Kornyliy Tretyak[1]*[0000-0001-5231-3517], Svitlana Nesterenko[1][0000-0002-2288-3524], Yuriy Bisovetskyi[2]

[1] Lviv Polytechnic National University, Lviv, Ukraine
[2] PJSC «Ukrhydroenergo», Vyshgorod, Kyiv region, Ukraine
*kornel1958@gmail.com

Abstract. The article examines the combined use of satellite radar and stationary systems for monitoring spatial displacements of structures (SSMSDS) to detect vertical deformations of dams. The object of research is the dam of the Kaniv HPP in Ukraine. Dam deformation monitoring includes automated use of GEOMOS software, as well as a GNSS and TPS points network. DInSAR radar interferometry algorithms were applied to calculate the vertical displacements of the dam based on satellite observations. This study analyzed 30 satellite images from Sentinel-1, taken every 12 days from August 10th, 2020 to August 5th, 2021. The error in determining the vertical movement speed of the dam control points is based on the data of radio interferometric measurements relative to the results obtained from GNSS and linear-angular measurements for the period from August 2020 to February 2021. The error margin was found to be 0.41 mm/mo, with an average speed of -3.5 mm/mo during that period. From February 2021 to August 2021, the error margin increased to 0.85 mm/mo, with an average speed of +1.7 mm/mo. Combining radar and ground measurements confirmed the seasonal spatiotemporal distribution of the rates of vertical dam displacements, with the dam body subsiding from August 2020 to February 2021 and then rising from February 2021 to August 2021. The radar measurements also identified anomalous speed zones with no GNSS points or reflectors for linear-angular measurements, which could indicate hidden defects related to the dam's strength. Overall, the results showed the effectiveness of using DInSAR technology and ground-based automated systems to monitor potentially dangerous objects, such as dams.

Keywords: deformation monitoring, vertical displacements, GNSS measurements, TPS measurements, differential interferometry (DInSAR), dam.

1. Introduction

The territory of Eastern Ukraine is saturated with potentially dangerous industrial facilities and areas whose geodynamic processes require constant control and monitoring to detect deformations. With the beginning of the full-scale invasion of Ukraine, man-made territories appeared in the danger zone. Military actions and aggression on a vast territory lead to numerous man-made and ecological disasters. Technogenic threats to energy facilities and hydrotechnical structures are especially dangerous. As a result of long-term operation, most large dams in the territory of Ukraine are prone to aging processes. Moreover, these engineering structures are periodically subjected to extreme loads from missile attacks.

In this regard, it is essential to monitor HPP dams, in particular by geodetic and geotechnical methods. In the conditions of war, remote methods are especially relevant. To date, some Ukrainian hydropower dams have installed systems for continuous monitoring of their displacements and deformations (Horb, 2023). These systems are built on the basis of the use of GNSS receivers and robotic total stations with automatic recognition of reflectors (TPS) and geotechnical sensors (deformographs, gap meters, inclinometers). The measurement results have a point spatial distribution. However, not all elements can be covered by these measurements, since the dam is comprised of separate concrete blocks and is connected to earthen dams. The monitoring systems for dams use GNSS receivers, robotic total stations, and geotechnical sensors to measure spatial distribution. Traditional geodetic methods like high-precision leveling, GNSS, TPS measurements, and measurement of Straightness are used to periodically monitor spatial displacements and deformations of soil dams within 3-12 months. However, this approach does not provide continuous spatial information and a satisfactory frequency of measurements over time. To address these shortcomings, the results of automated systems for monitoring displacements and deformations are combined with remote sensing using interferometric synthetic aperture radar (InSAR) for a comprehensive analysis of hydroelectric dams under extreme conditions. The reliability and accuracy of the joint processing of geodetic radar measurements are assessed in this study.

2. Page layout

When monitoring technogenic areas, traditional ground geodetic methods have limitations due to a small number of ground points and difficulties in adverse weather conditions (Carlà 2019). However, remote shooting methods have improved geospatial data collection technology, increasing accuracy and efficiency. SAR satellites and radar interferometry are crucial tools in monitoring ground surface movements, as well as minor displacements in structures

like dams, buildings, and bridges (Perissin 2016). Radar observations can be conducted at any time of day (Graham 1974) and are not affected by cloudiness or insufficient lighting (Perissin 2016). With satellite technology, the displacement of Earth's surface can be determined accurately from a centimeter to a millimeter (Rosen 2000).

In recent years, automated data processing methods have demonstrated significant improvements in processing SAR images. In fact, they even surpass traditional geodetic methods in terms of accuracy (Passah et al. 2023). InSAR technology allows for dynamic evaluation of objects under study, providing displacement maps that can be remotely analyzed. Satellite interferometry with a synthesized aperture (InSAR) is particularly useful in studying landslides on a global, local, or regional scale (Colesanti et al. 2006). Changes in the vertical and horizontal position of a network of points caused by hydrometeorological, geological, hydrological, and other factors, including man-made territories, can be detected. This is particularly relevant for hydropower plants, which often cover river valleys affected by endogenous and exogenous processes. It is crucial to choose the right radar image processing method to determine the displacement of large engineering objects, such as hydraulic structures.

(Aswathi 2022) presents a general overview of the possibility of using InSAR, including monitoring hydropower facilities. Among the listed methods of remote sensing, we selected those that are most widely used and approved by other researchers. Persistent Scatterer Interferometry PSInSAR (Ferretti 2011; Bouali et al. 2017) is suitable for determining the deformation of artificial structures and other stable points. Persistent scatterer (PS), which is used to identify pixels, is a ground-based specially installed radar target that has a constant high value of reflectivity for a long time period. Distributed Scatterer Interferometry DS-InSAR (Flores-Anderson 2019) uses a dense ground network of distributed scatterer (DS), i.e. natural radar targets that have a radar signature and reflectivity similar to PS. The method is convenient for determining deformations in forested regions, as well as for assessing soil deformation. Small Baseline Subset SBAS (Vajedian 2015) generates vector maps of average strain rate and displacement time series for the study area based on the small baseline subset technique using points with defined coordinates. The Multi-temporal Satellite-based Differential Interferometry MTInSAR combines either PS and DS methods (Xiong et al. 2019), or PS and SBAS methods (Fárová 2019). The deformation field is obtained by phase calculation and time series analysis. Time Series Interferometric Synthetic Aperture Radar TS-InSAR (Cao 2018) detects slow strain rates by examining phase changes in SAR images acquired by low-carrier sensors. Displacement along the installed scatterers leads to the automatic interpretation of dam deformation scenarios. The application of TS-InSAR, PSInSAR, DS-InSAR, and SBAS methods, provides the technological selection of points (pixels) with high coherence and consistency of time series on SAR images. They also determine the dynamics and direction of scatterer displacements. Combined MTInSAR has the greatest advantages for the study of engineering structures, as the time series of the displacement along the installed scatterers leads to the automatic interpretation of dam deformation scenarios.

Several scientific publications have reported on the successful application of PSInSAR technology in analyzing dam deformation. Wang et al. (2011) used this technology to study the Three Gorges Dam area in China on the Yangtze River, while Vázquez-Ontiveros et al. (2023) studied the Sanalona Dam in Mexico. The results obtained through PSInSAR were consistent with traditional geodetic methods and GNSS measurements. Additionally, Pang et al. (2023) confirmed the effectiveness of SBAS-InSAR technology in studying vertical displacements of the Banqiao Reservoir Dam surface in China between 07/03/22 and 08/20/22. The dam displacement fluctuated between 4 to -8 mm, with the largest deviations between InSAR and GNSS (BeiDou) monitoring values being 2 mm. In another study by Liu et al. (2021), two methods of remote monitoring, namely distributed scatterer DS-InSAR, and SBAS-InSAR, were used to study the deformation of the Xiaolangdi Dam. The results obtained through cross-validation showed that the different InSAR methods produced identical results. Xiong et al. (2019) used MTInSAR technology to monitor the Chang Lingpi Dam and found that the maximum deformation rates of the dam crest monitoring points were up to -30 mm/year, with discrepancies between radar interferometry and ground geodetic measurements not exceeding 2.1 mm/year. Finally, the TS-InSAR method (Xiao and He 2019; Xiao et al. 2022) was applied to study the sudden subsidence of the Sardoba Reservoir in Uzbekistan, which was found to be up to 60 mm. Timely verification by ground methods helped avoid a significant man-made disaster.

The advantage of the listed methods lies in the high accuracy of measurements. However, these methods require the installation of special reflectors (PS), which complicates the process of remote monitoring of objects, especially in hard-to-reach places. To obtain a continuous field of deformations, it is advisable to use the method of Differential Interferometry DInSAR (e.g., Crosetto et al., 2011). DInSAR makes it possible to study large flat surfaces. It provides a spatial picture of deformations, thus increasing the safety of technogenic territories, and preventing the disaster. DInSAR is a classical data processing method. Undoubtedly, the combined use of DInSAR with the PSInSAR method in the presence of PS is the best option for monitoring engineering structures. This significantly increases the accuracy and reliability of monitoring the deformations of potentially dangerous objects and their adjacent territories (Fárová 2019).

The application of the DInSAR method has a number of advantages. This method provides remote measurements of relatively small deformations within large areas of the Earth's surface. This helps to detect displacements in regions where deformations are difficult to measure with classical ground geodetic methods. It also allows for achieving results both with lower labor costs and cost indicators.

The differential method has limitations in urbanized areas with high buildings, in forested and snowy areas. In such cases, ambiguous results may occur, including changes in the display of objects or zones, the appearance of shadows, and signal interference (Herrera 2013). The most important limitation of DInSAR is the loss of coherence. This parameter characterizes the correlation of the values of the main and auxiliary images. If the coherence value is close to one, it means that the signal-to-noise ratio for the interference pattern is satisfactory. In order to get reliable strain estimates, the phase of the interferometric signal needs to be satisfactory. Coherent pixels or PSs are the pixels that meet this requirement and are often used in DInSAR (Crosetto 2011).

Numerous scientific studies have confirmed that the DInSAR method is effective in determining dam deformations compared to other terrestrial methods. The movement of the Conza Dam in Italy, located in an active seismic zone, was observed using 40 images of the Envisat-ASAR satellite from 2004 to 2010. The results were compared to the data from extensometers, and both monitoring systems provided similar dam subsidence values of 65 mm with a maximum deviation of 4.5 mm between SAR and USBR measurements. DInSAR is highly sensitive in detecting minor deformations, as seen in the monitoring results of the Campolattaro Dam in Italy using Sentinel-1A images, which recorded subsidence of the dam within 1-2 mm and were confirmed by high-precision leveling results (S.L. Ullo 2019). Quite satisfactory results can be obtained even when using images with a low resolution, up to 100 m. The stability of the Taiho Subdam in Okinawa Prefecture, Japan was confirmed through the use of images from the Japanese satellite ALOS PALSAR (K. Honda et al. 2012). The dam experienced vertical displacements of 89.1 mm (DInSAR) and 104.2 mm (GPS) between 2006 and 2010, as well as 0.8 mm (DInSAR) and 3.4 mm (GPS) between 2008 and 2009. Satellite radar technologies, especially DInSAR, allow for the use of accumulated databases of radar images to inspect and clarify the deformation processes of dams from past years. The combination of archival instrumental surveys from 1975-1980 and DInSAR from 1995-2010 was used to identify a long-term deformation process in the La Pedrera reservoir dam in SE Spain, providing a complete non-uniform spatiotemporal view of displacements in the dam that was impossible to detect through ground instrumental measurements. The InSAR method is useful for determining displacement with high accuracy when deformations are slow, and unknown dynamics can be detected thanks to a fairly high frequency of repeated images. This was demonstrated in a study by Joaquim et al. in 2016 (Joaquim et al. 2016).

After conducting research on various dams across the world, it was discovered that satellite SAR interferometry methods can be used to observe movements in dam structures. Through long-term monitoring of dams using the DInSAR method, it is possible to achieve accurate results in determining deformations that are on par with terrestrial geodetic methods. However, this method is most effective when monitoring slow deformations over time and when combining the results with ground geodetic measurements. The only drawback of this method is that the reliability of the results is dependent on weather conditions. In our particular case, we utilized the DInSAR technology to determine surface deformations of the Kaniv HPP, which is located on the Dnipro River near the northern outskirts of the city of Kaniv in the central part of Ukraine (Fig. 1).

Fig. 1 Location of the Kaniv HPP

The construction of hydropower facilities was carried out mainly from 1967 to 1975. The reservoir was filled from 1972 to 1978. The main structures and nodes of the hydroelectric power station include: 1) right-bank earthen dam; 2) gateway; 3) HPP building with a concrete dam; 6) left-bank earthen dam. The concrete part of the dam is divided by expansion joints into six sections with a length of 57.00 m each. The length of the pressure front of the hydroelectric unit is 16.30 km, and the maximum water level difference between the upper and lower beif is 12 m. The general appearance of the HPP structures is shown in the photo (Fig. 2).

The HPP building and the first section of the dam, sections 2-6 of the dam,

Fig. 2 General view of the Kaniv HPP and geological zoning of the dam

The buildings located on the soil massif are subject to complex engineering and geological conditions. The geological structure consists of a complex of Quaternary sediments, including the floodplain alluvial formation, the Shevchenko Formation, and the buried moraine layer. The concrete construction node is divided into two areas based on engineering and geological conditions: the HPP building and the first section of the dam, and the second to sixth sections of the dam. The first section of the dam has a high deposit of moraine, with an uneven roof that lies at absolute elevations ranging from +43,000 to +62,000 m. In the second section, the sand layer at the base is several tens of meters thick and contains numerous layers and lenses of clay soils. To ensure a sturdy foundation, poor-quality foundation soils in the HPP building and most of the dam are deepened to a depth of 3-4 m and replaced with clean sand. Each section houses four horizontal hydro units with generators with a capacity of 17.50 MW, and the height of the dam from the base to the top of the crane beam is 39.70 meters.

To control the displacements and deformations of the Kaniv HPP dam, a stationary monitoring system for spatial displacements of structures (SSMSDS) was implemented. The SSMSDS is a hardware and software complex designed to perform periodic precision measurements by GNSS receivers and robotic electronic total stations (TPS) to determine the coordinate-time location of geodetic points fixed on the surface of the dam. It includes geodetic pylons with GNSS receivers, robotic electronic total stations, communication and computer equipment, and specialized software that operates continuously.

Geodetic points of SSMSDS are divided into reference and control points. Reference points are designed to assess the influence of geodynamic factors on the network of control points. The reference points of the SSMSDS of the Kaniv HPP are KNR1 and KNR2 points located farthest from the concrete dam (Fig. 3), which are fundamental geodetic points equipped with a GNSS receiver Leica GMX902 GG with an AR10 antenna, a Leica Total Stations (TPS) TM30 robotic total station (Fig. 4a).

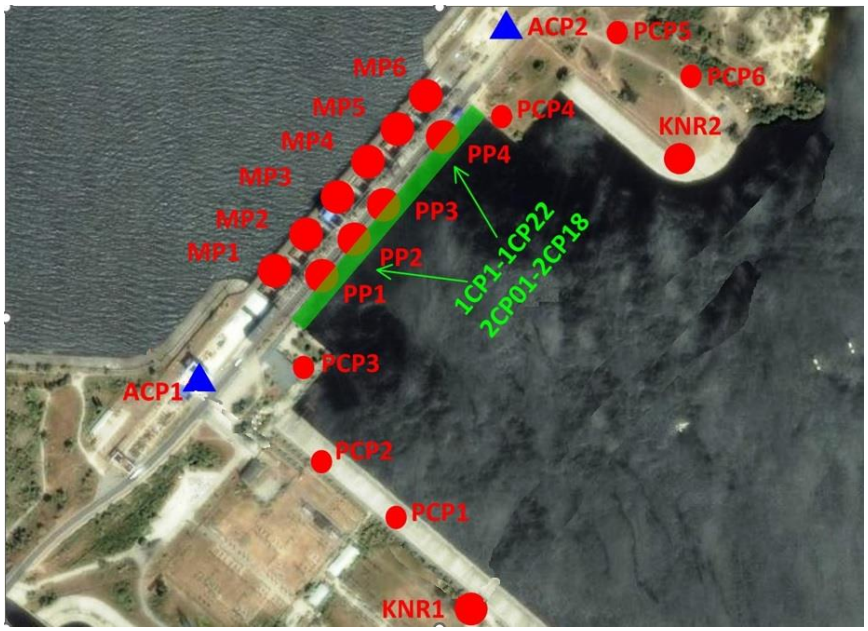

Fig. 3 The network of geodetic points of the SSMSDS of Kaniv HPP

a b c

Fig. 4 General view of geodetic points of SSMPPSS of Kaniv HPP
a) KNR1, KNR2; b) MP1 – MP6 i ACP2; c) PP1 – PP4 i ACP1

Control points of SSMSDS of the Kaniv HPP are divided into GNSS points and TPS points. GNSS points are equipped with Leica GMX902 GG GNSS receivers with an AR10 antenna and a reflector for TPS measurements (Fig. 4, b). These include points MP1 - MP6, PP1 - PP4, ACP1, and ACP2, the coordinates of which are determined on the basis of GNSS and linear-angular measurements (Fig. 3). TPS points are equipped only with reflectors for TPS measurements (Fig. 4, c). These include points 1CP1 – 1CP22, 2CP01 – 2CP18, and PCP1 – PCP6 (46 points), the coordinates of which are determined only on the basis of linear and angular measurements.

The measurements of the SSMSDS are conducted continuously with a frequency of 30 seconds, while TPS measurements with a frequency of 6 hours are performed from reference points to control points equipped with

reflectors. The GEOMOS software is used to determine the coordinates of all control points of the SSMSDS every 6 hours, which are then averaged for each day. The stability of the reference points KNR1 and KNR2 is assessed based on the results of daily GNSS measurements processed by the BERNESE software (http://www.bernese.unibe.ch/). A detailed analysis of the results of GNSS and TPS measurements revealed seasonal horizontal and vertical fluctuations of all control points, with extreme values of displacements occurring almost every year in the first decade of February and August. This regularity can be observed at all dams of Ukraine equipped with SSMSDS. The reason for these seasonal opposite shifts is the temperature deformation of the dam (Tretyak and Palianytsia 2022). It is important to note that seasonal deformations of the dam are confirmed by the data of joint processing of geodetic and geotechnical sensors (Tretyak, Zayats and Hrabovyi 2023). Displacement occurs according to a linear law within seasonal periods (Tretyak and Palianytsia 2021), and it is necessary to consider the linear displacement speeds of control points within these periods. The semiannual change in the direction of the vectors of vertical displacements of control points leads to an annual fluctuation of the dam by up to 20 mm per year. The measurements of the SSMSDS are conducted continuously with a frequency of 30 seconds, while TPS measurements with a frequency of 6 hours are performed from reference points to control points equipped with reflectors. The GEOMOS software is used to determine the coordinates of all control points of the SSMSDS every 6 hours, which are then averaged for each day. The stability of the reference points KNR1 and KNR2 is assessed based on the results of daily GNSS measurements processed by the BERNESE software. A detailed analysis of the results of GNSS and TPS measurements revealed seasonal horizontal and vertical fluctuations of all control points, with extreme values of displacements occurring almost every year in the first decade of February and August. This regularity can be observed at all dams of Ukraine equipped with SSMSDS. The reason for these seasonal opposite shifts is the temperature deformation of the dam. It is important to note that seasonal deformations of the dam are confirmed by the data of joint processing of geodetic and geotechnical sensors. Displacement occurs according to a linear law within seasonal periods, and it is necessary to consider the linear displacement speeds of control points within these periods. The semiannual change in the direction of the vectors of vertical displacements of control points leads to an annual fluctuation of the dam by up to 20 mm per year.
For example, Fig. 5 presents a time series of vertical displacements of control GNSS point MP1. It can be seen from this figure that the extremes of displacement occur every year in February and August.

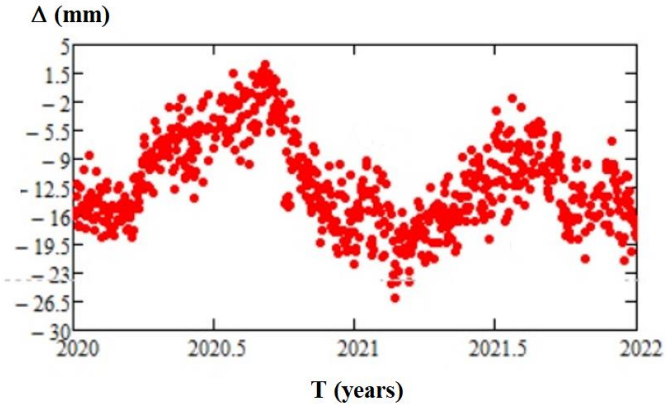

Fig. 5 Time series of height displacements of the MP1 reference GNSS point

To compare the vertical displacements of SSMSDS, we used radio interferometric images from the period between 2020.6 and 2021.6. During this time, we compared the results of daily GNSS and TPS measurements with radar images from the Sentinel-1 satellite taken every 12 days. Tables 1 and 2 show the vertical velocities of GNSS and TPS control points for the periods between (2020.6-2021.1) and (2021.1-2021.6). The accuracy of speed determination for most control points is almost ten times smaller than their values, as shown in Tables 1 and 2.

Table 1 Vertical movement speeds of GNSS control points for the period from 2020.6 to 2021.6

POINT	PERIOD			
	2020.6 – 2021.1		2021.1 – 2021.6	
	V_U, (mm/mo)	M_{VU}, (mm/mo)	V_U, (mm/mo)	M_{VU}, (mm/mo)
ACP1	-1.9	0.4	0.7	0.3
ACP2	0.1	0.4	-0.8	0.3
MP1	-4.1	0.4	3.1	0.3
MP2	-3.8	0.4	2.8	0.3
MP3	-3.9	0.4	2.6	0.3

MP4	-3.2	0.4	2.4	0.3
MP5	-3.7	0.4	2.2	0.4
MP6	-3.5	0.4	2.5	0.4
PP1	-3.3	0.5	0.6	0.5
PP2	-4.2	0.4	3.0	0.4
PP3	-1.6	0.5	-0.3	0.5
PP4	-1.5	0.3	*	*

Note: * Data is missing due to a malfunction of the GNSS receiver.

Table 2 Vertical movement speeds of TPS control points for the period from 2020.6 to 2021.6

POINT	PERIOD				POINT	PERIOD			
	2020.6 – 2021.1		2021.1 – 2021.6			2020.6 – 2021.1		2021.1 – 2021.6	
	V_U, (mm/mo)	M_{VU}, (mm/mo)	V_U, (mm/mo)	M_{VU}, (mm/mo)		V_U, (mm/mo)	M_{VU}, (mm/mo)	V_U, (mm/mo)	M_{VU}, (mm/mo)
1KCP1	-2.9	0.2	1.4	0.4	1KMP19	-3.4	0.3	1.4	0.3
1KCP2	-0.9	0.2	-0.9	0.4	1KMP2	-2.8	0.1	0.6	0.3
1KM1	-2.2	0.1	1.1	0.1	1KMP20	-3.1	0.3	1.4	0.3
1KM2	-2.4	0.1	0.8	0.2	1KMP21	-3.4	0.3	1.7	0.3
1KMP10	-3.1	0.2	1.3	0.3	1KMP22	-3.3	0.3	1.6	0.3
1KMP11	-3.7	0.2	1.5	0.3	1KMP4	-2.8	0.1	0.3	0.4
1KMP12	-3.6	0.2	1.7	0.3	1KMP7	-3.1	0.2	0.4	0.4
1KMP13	-3.6	0.1	1.4	0.3	1KMP8	-3.5	0.1	1	0.4
1KMP14	-3.6	0.2	1.2	0.3	1KMP9	-3.6	0.2	1.1	0.4
1KMP15	-3.5	0.2	1.5	0.3	1KPP1	-3	0.3	2.6	0.3
1KMP16	-3.8	0.1	1.7	0.3	1KPP2	-3.6	0.1	2.4	0.3
1KMP17	-3.9	0.2	1.8	0.3	1KPP3	-4.1	0.2	2.2	0.3
1KMP18	-3.6	0.2	1.7	0.3	1KPP4	-2.9	0.2	1.4	0.3

Figs. 4 - 5 present the spatial distribution of vertical displacements of GNSS and TPS points for the periods (2020.6 - 2021.1) and (2021.1 - 2021.6). Fig. 6 reveals that the vertical velocities of points are distributed uniformly within the concrete part of the dam. However, the velocities of points on the land side of the dam (GNSS control points ACP-1, ACP-2, and TPS points 1KM1, 1KM2, 1KCP1, 1KCP2) are significantly lower. This is obviously related to the temperature deformation of the concrete part of the dam. According to the results of measurements in the period (2021.1 - 2021.6) (Fig. 7), on the concrete part of the dam, the vertical displacement velocities of the GNSS control points are uniform, but for the TPS points, the spatial distribution of velocities is more uneven. This could be a result of defects in the strength of the dam structures against temperature deformations when the southern side of the dam, on which the TPS reflectors are located, is heated. Similarly, as in the previous period, the velocities of points located on the land side of the dam are significantly smaller in magnitude.

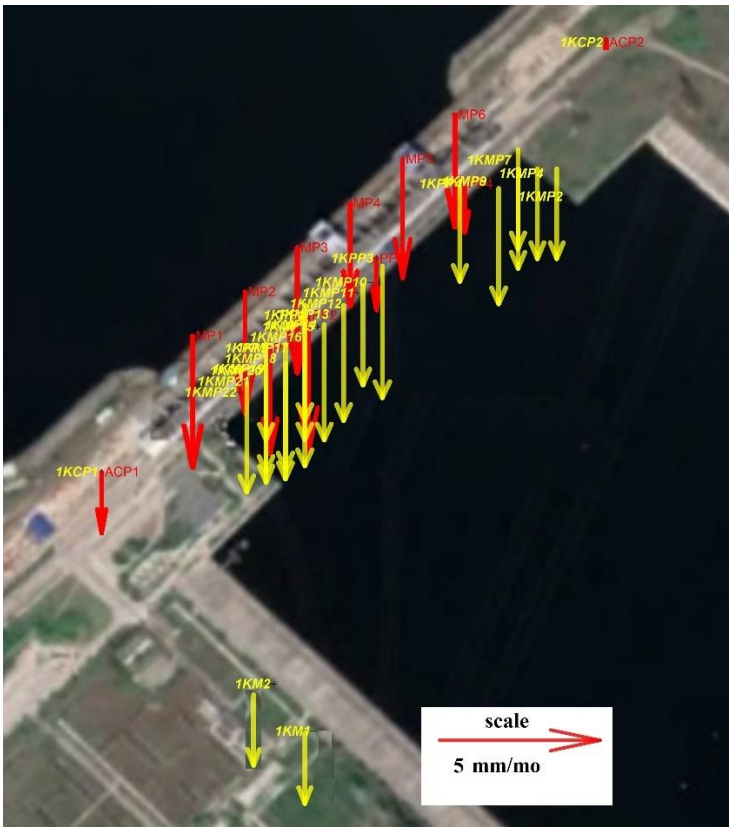

Fig. 6 Scheme of vertical velocity displacement vectors of control points of the linear-angular network of SSMSDS at Kaniv HPP for the period from 2020.6 to 2021.1. (→ GNSS point displacement velocity vector, → TPS linear-angular network point displacement velocity vector

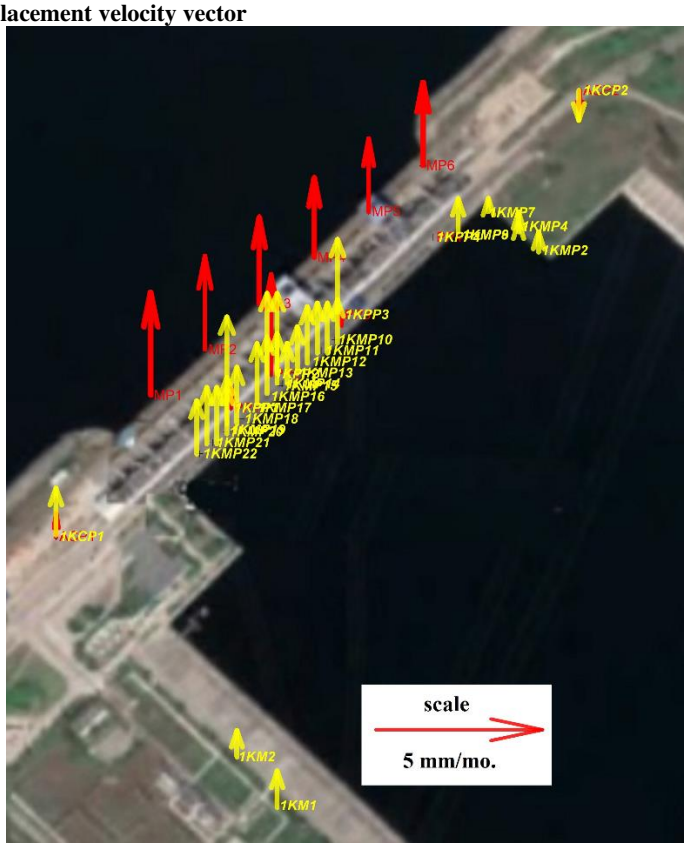

Fig. 7 Scheme of vertical velocity displacement vectors of control points of the linear-angular network of SSMSDS at Kaniv HPP for the period from 2021.1 to 2021.6. (→ GNSS point displacement velocity vector, → TPS linear-angular network point displacement velocity vector

Methodology

Using the DInSAR technology on satellite radar, the Kaniv HPP dam's surface deformations were studied. The research was conducted on the Linux platform's SNAP software, which is freely available, by using radar images captured by the Sentinel-1 satellite (http://step.esa.int/downloads/6.0/installers/esa-snap_all_unix_6_0.sh). These images were uploaded to the Copernicus Open Access Hub web platform (https://scihub.copernicus.eu/). Differential interferometry is the technique used to create a differential interferogram, which quantifies and reflects the earth's surface movement between two epochs of shooting (Massonnet et al. 1998). After removing the topographic effect, the phase component of two SAR images is differentiated to calculate the displacement. One image is taken at the initial measurement epoch, while the other is taken at the next measurement epoch. The construction of a vertical displacement map involves three stages: Co-Registration, the construction of a differential interferogram, and the formation of a vertical displacement map. The TOPS module is used for the coregistration of Sentinel-1 images obtained by TOPSAR technology to form an interferogram (Yagüe-Martínez et al. 2016). The resulting data is exported to the SNAPHU plugin, which is used to unfold a filtered interferogram, resulting in an image with certain distortions (Chen et al. 2003). The expanded results should be interpreted as the relative vertical displacements between the pixels of the two images. The data obtained after the deployment of the phase is loaded again into SNAP and the removal of geometric distortions is performed. Then the accuracy of the data is checked. As a result, we get an offset in the direction of the straight line that connects the satellite radar to the point on the ground surface (LOS). Positive values of LOS displacements mean movement of the surface in the direction of the radar (rising), and negative values - movement away from the radar (lowering). The final stage is the geocoding of the height matrix, that is, the conversion of phase values into height and the transformation of the displacement map into a geographic coordinate system. The study processed 31 satellite images received by the Sentinel-1 satellite from August 10, 2020, to August 5, 2021, received every 12 days (Table 3).

Table 3 Information on Sentinel-1 satellite images used for research

Date	ORBIT_CYCLE	REL_ORBIT	ABS_ORBIT	Date	ORBIT_CYCLE	REL_ORBIT	ABS_ORBIT
10.08.2020	137	87	22863	18.02.2021	153	87	25663
22.08.2020	138	87	23038	02.03.2021	154	87	25838
03.09.2020	139	87	23213	14.03.2021	155	87	26013
15.09.2020	140	87	23388	26.03.2021	156	87	26188
27.09.2020	141	87	23563	07.04.2021	157	87	26363
09.10.2020	142	87	23738	19.04.2021	158	87	26538
21.10.2020	143	87	23913	01.05.2021	159	87	26713
02.11.2020	144	87	24088	13.05.2021	160	87	26888
14.11.2020	145	87	24263	25.05.2021	161	87	27063
26.11.2020	146	87	24438	06.06.2021	162	87	27238
08.12.2020	147	87	24613	18.06.2021	163	87	27413
20.12.2020	148	87	24788	30.06.2021	164	87	27588
01.01.2021	149	87	24963	12.07.2021	165	87	27763
13.01.2021	150	87	25138	24.07.2021	166	87	27938
25.01.2021	151	87	25313	05.08.2021	167	87	28113
06.02.2021	152	87	25488				

Based on the results of processing satellite images, a time series of its vertical displacement was determined for each pixel (10x10 m). For example, Fig. 8 presents the time series of the vertical displacement of one of the points located near the MP2 GNSS point determined by radar interferometry data. It can be seen from this figure that during the period from 2020.6 to 2021.1, there is a subsidence of the point $\Delta \approx$ -40 mm, and during the period from 2021.1 to 2021.6, on the contrary, there is a rise of the point by approximately the same amount. This is evidenced by the trend lines plotted on the time series. Practically all points determined on the dam have similar trends, which coincide with the data of GNSS stations and TRS measurements.

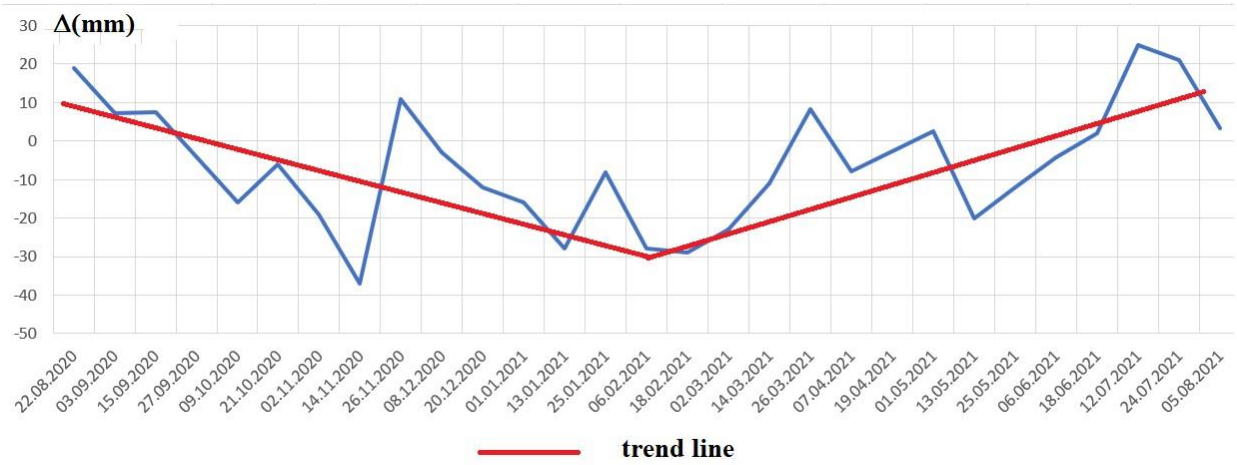

Fig. 8 The time series of vertical displacements of one of the points located near the MP2 GNSS point, determined by radar interferometry data

The construction of displacement maps in relation to the initial date has revealed some unusual vertical displacement values in certain satellite images. For instance, in Fig. 9 in the epoch from 2020.6 to 2020.9, a significant subsidence of the dam was detected, which is not typical for the time series. To identify the reasons for this, we decided to examine the meteorological characteristics of the atmosphere in this area on those dates (https://meteopost.com/weather/archive/). Precipitation was recorded in three images: 14th November 2020, 7th April 2021, and 13th May 2021. The presence of precipitation distorts the image on the displacement maps, and it affects the quality of the measurement results due to the influence of atmospheric processes and weather conditions. Monitoring deformations under adverse conditions can cause errors in the obtained results, and this problem is further exacerbated by prolonged periods of precipitation.

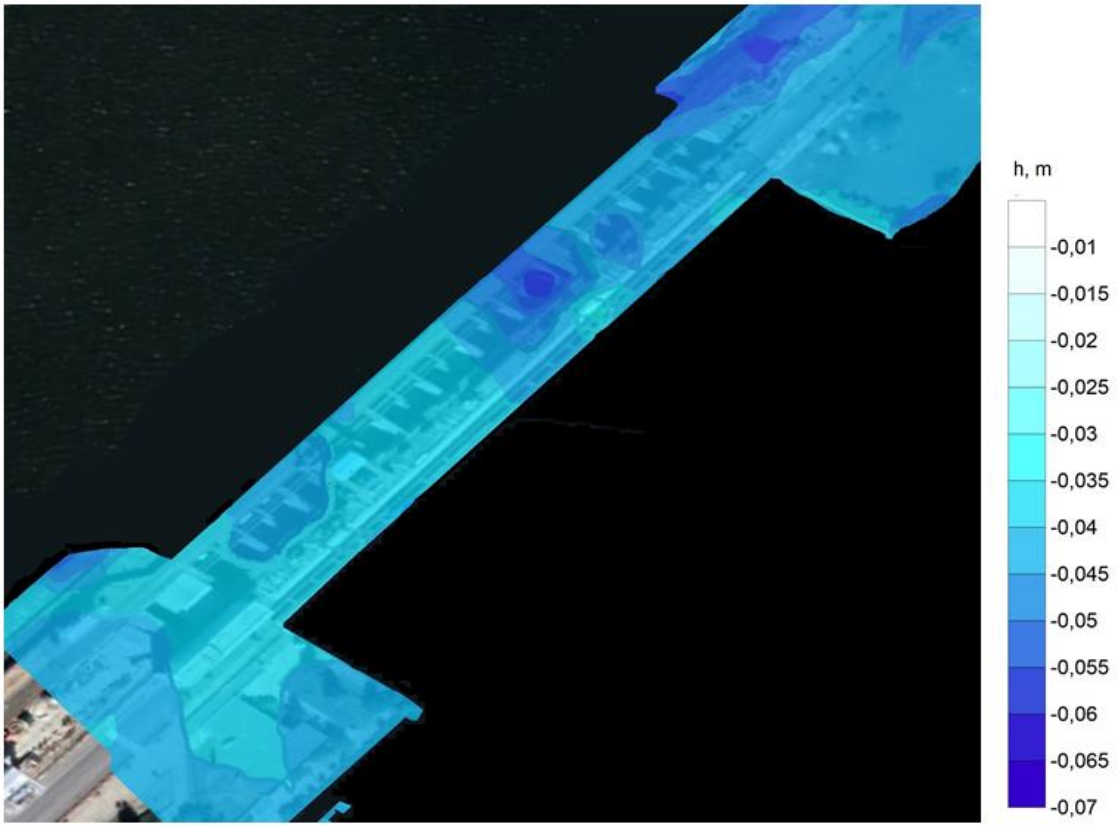

Fig. 9 Map of vertical displacements for the period 08.10.20 - 11.14.20

For the entire area of the dam, based on the results of processing radar images using the DInSAR method, the linear velocities of vertical displacements for two periods (2020.6 - 2021.1), (2021.1 - 2021.6) were determined for each pixel. Table 4 shows, a fragment of the data array presenting the results of determining the vertical velocities. It also demonstrates an assessment of the accuracy of the dam points' movement (pixel size 10x10 m).

Table 4 Fragment of the array of data on the determination of the vertical velocities of the dam points for the periods 2020.6 – 2021.6, 2021.6 – 2022.1

$X_{(M)}$	$Y_{(M)}$	TIME PERIOD			
		2020.6 – 2021.1		2021.1 – 2021.6	
		V (mm/mo)	M_V (mm/mo)	V (mm/mo)	M_V (mm/mo)
262.21	3.60	-4.1	2.0	3.5	1.3
261.25	9.28	-4.4	2.0	3.8	1.4
260.17	15.67	-4.6	2.0	3.9	1.4
259.09	22.07	-4.7	2.0	4.2	1.3
258.02	28.46	-4.8	2.0	4.3	1.3
256.94	34.85	-5.0	2.0	4.2	1.3
255.86	41.25	-5.1	2.0	4.3	1.4
254.78	47.64	-5.3	1.9	4.3	1.4
253.71	54.04	-5.6	1.9	4.4	1.3
252.63	60.43	-5.6	1.9	4.4	1.3

Tables 5 - 6 present the results of determining the vertical movement speeds of the control points of the dam for the periods (2020.6 - 2021.1 and 2021.1 - 2021.6) based on GNSS, linear-angular, and radio interferometric measurements. The given vertical velocities according to DInSAR data correspond to the nearest pixel located relative to the control point. Tables 5 – 6 show the speed differences determined by the results of radio interferometric measurements and GNSS or linear-angular measurements.

$$\Delta = V_{DinSar} - V_{(GNSS\ or\ TPS).} \quad (1)$$

Table 5 Results of determining the vertical speeds of movement of dam`s control points for the period (2020.6 - 2021.1) according to GNSS, linear-angular and radio interferometric measurements

Control points	$X_{(M)}$	$Y_{(M)}$	$V_{(GNSS\ OR\ TPS)}$ (mm/mo)	V_{DInSAR} (mm/mo)	Δ (mm/mo)	$V_R = V_{DInSAR} - \Delta_{AVG}$ (mm/mo)	$\Delta R = \Delta - \Delta_{AVG}$ (mm/mo)
MP1	215.57	24.07	-4.1	-4.7	-0.6	-3.5	0.6
MP2	252.25	67.61	-3.8	-5.4	-1.6	-4.2	-0.4
MP3	289.00	111.15	-3.9	-5.2	-1.3	-4	-0.1
MP4	325.92	154.88	-3.2	-4.4	-1.2	-3.2	-0
MP5	362.71	198.50	-3.7	-4.8	-1.1	-3.6	0.1
MP6	399.48	242.01	-3.5	-3.7	-0.2	-2.5	1
PP1	205.45	88.20	-3.3	-5.3	-2.0	-4.1	-0.8
PP2	232.78	120.47	-4.2	-5.1	-0.9	-3.9	0.3
1KCP1	102.65	-51.63	-2.9	-3.9	-1.0	-2.7	0.2
1KM1	-112.55	124.54	-2.2	-3.7	-1.5	-2.4	-0.2
1KM2	-73.48	91.40	-2.4	-3.7	-1.3	-2.4	-0
1KMP10	260.14	171.34	-3.1	-4.6	-1.5	-3.3	-0.2
1KMP11	251.41	160.98	-3.7	-4.8	-1.1	-3.5	0.2
1KMP12	242.55	150.49	-3.6	-5.0	-1.4	-3.8	-0.2
1KMP13	233.58	139.86	-3.6	-5.2	-1.6	-3.9	-0.3
1KMP14	224.93	129.62	-3.6	-5.2	-1.6	-4	-0.4
1KMP15	223.28	127.60	-3.5	-5.2	-1.7	-4	-0.5
1KMP16	214.61	117.36	-3.8	-5.2	-1.4	-4	-0.2
1KMP17	205.62	106.69	-3.9	-5.1	-1.2	-3.8	0.1
1KMP18	196.81	96.26	-3.6	-5.0	-1.4	-3.8	-0.2
1KMP19	188.13	85.96	-3.4	-4.9	-1.5	-3.6	-0.2
1KMP2	331.54	334.09	-2.8	-4.1	-1.3	-2.9	-0.1
1KMP20	186.59	84.16	-3.1	-4.8	-1.7	-3.5	-0.4
1KMP21	177.78	73.71	-3.4	-4.3	-0.9	-3.1	0.3
1KMP22	168.97	63.26	-3.3	-4.3	-1.0	-3.1	0.2
1KMP4	350.70	317.95	-2.8	-4.4	-1.6	-3.2	-0.4
1KMP7	361.80	291.80	-3.1	-4.2	-1.1	-2.9	0.2
1KMP8	343.99	270.70	-3.5	-4.2	-0.7	-3	0.5
1KMP9	343.99	270.70	-3.6	-4.2	-0.6	-3	0.6
1KPP3	280.17	176.76	-4.1	-4.5	-0.4	-3.3	0.8

1KPP4	342.14	249.95	-2.9	-4.5	-1.6	-3.3	-0.4

Table 6 Results of determining the vertical speeds of movement of the dam`s control points for the period (2021.1 - 2021.6) according to GNSS data, linear-angular and radio interferometric measurements

Control points	$X_{(M)}$	$Y_{(M)}$	$V_{(GNSS\ OR\ TPS)}$ (mm/mo)	V_{DInSAR} (mm/mo)	Δ (mm/mo)	$V_R = V_{DInSAR} - \Delta_{AVG}$ (mm/mo)	$\Delta R = \Delta - \Delta_{AVG}$ (mm/mo)
ACP1	102.65	-51.63	0.7	4.0	3.3	1.4	0.7
MP1	215.57	24.07	3.1	4.3	1.2	1.8	-1.3
MP2	252.25	67.61	2.8	4.4	1.6	1.9	-0.9
MP3	289.00	111.15	2.6	4.2	1.6	1.6	-1
MP4	325.92	154.88	2.4	3.6	1.2	1.1	-1.3
MP5	362.71	198.50	2.2	4.2	2.0	1.7	-0.5
MP6	399.48	242.01	2.5	4.3	1.8	1.7	-0.8
PP2	232.78	120.47	3	4.6	1.6	2	-1
1KCP1	102.65	-51.63	1.4	4.0	2.6	1.4	0
1KM1	-112.55	124.54	1.1	3.0	1.9	0.5	-0.6
1KM2	-73.48	91.40	0.8	3.3	2.5	0.8	-0
1KMP11	251.41	160.98	1.5	4.2	2.7	1.7	0.2
1KMP12	242.55	150.49	1.7	4.4	2.7	1.9	0.2
1KMP13	233.58	139.86	1.4	4.5	3.1	2	0.6
1KMP14	224.93	129.62	1.2	4.4	3.2	1.9	0.7
1KMP15	223.28	127.60	1.5	4.4	2.9	1.9	0.4
1KMP16	214.61	117.36	1.7	4.4	2.7	1.8	0.1
1KMP17	205.62	106.69	1.8	4.3	2.5	1.8	-0
1KMP18	196.81	96.26	1.7	4.4	2.7	1.9	0.2
1KMP2	331.54	334.09	0.6	3.8	3.2	1.3	0.7
1KMP20	186.59	84.16	1.4	4.4	3.0	1.9	0.5
1KMP21	177.78	73.71	1.7	4.2	2.5	1.6	-0.1
1KMP22	168.97	63.26	1.6	4.0	2.4	1.4	-0.2
1KMP4	350.70	317.95	0.3	5.2	4.9	2.7	2.4
1KMP7	361.80	291.80	0.4	4.4	4.0	1.9	1.5
1KMP8	343.99	270.70	1	4.6	3.6	2.1	1.1
1KPP1	205.46	88.21	2.6	4.6	2.0	2.1	-0.5
1KPP2	232.79	120.48	2.4	4.6	2.2	2	-0.4
1KPP3	280.17	176.76	2.2	3.8	1.6	1.3	-0.9

Tables 5 – 6 show that there are systematic components in the distribution of differences Δ. The average value of the differences Δ for the period (2020.6 – 2021.1) is $\Delta_{avg} = -1.23$ mm/mo with a standard deviation of Stdev = 0.41 mm/mo, and for the period (2021.1 – 2021.6) $\Delta_{avg} = +2.52$ mm/mo with a standard deviation of Stdev = 0.85 mm/mo. These variations in speed that occur regularly are caused by various factors, including temporal and spatial decorrelation, signal delay from tropospheric delays that are not corrected perfectly in InSAR data [Heresh Fattahi & Falk Amelung 2014], orbital or topographical errors (Pawluszek- Filipiak et al. 2020), and the shift in vertical velocities of points from the LOS coordinate system to WGS-84.

Tables 5 and 6 show the reduced vertical velocities determined from radio interferometric measurements with the systematic component removed

$$V_r = V_{DinSar} - \Delta_{avg}, \quad (2)$$

as well as reduced differences Δ_r

$$\Delta_r = \Delta - \Delta_{avg..} \quad (3)$$

Figs. 10 and 11 present bar charts of the distribution of reduced differences Δ_r. For the period (2020.6 – 2021.1) most values of Δ_r are in the range of $-0.5 \div +0.3$ mm/mo, and for the period (2021.1 – 2021.6) they are in the range of $-1.1 \div +0.8$ mm/mo.

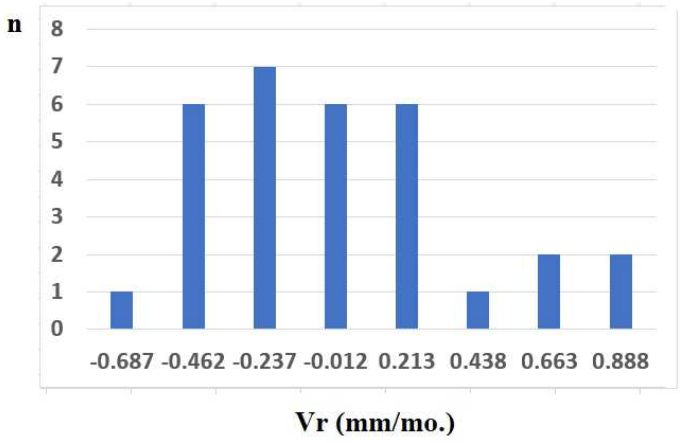

Fig. 10 Bar chart of the distribution of reduced differences Δ_r for the measurement period (2020.6 – 2021.1)

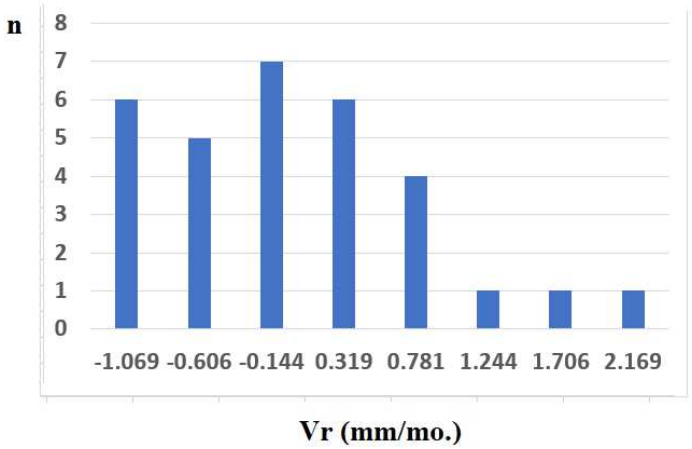

Fig. 11 Bar chart of the distribution of reduced differences Δ_r for the measurement period (2021.1 – 2021.6)

According to the data of reduced vertical velocities determined from radio interferometric measurements, schemes of their spatial distribution were constructed for two periods (2020.6 – 2021.1) and (2021.1 – 2021.6). As can be seen from Figs. 12 and 13, the spatial distribution of deformation rates of the dam surface is uneven. A common area is highlighted on both maps, where there is a field of maximum deformation rates. GNSS points and reflectors for linear and angular measurements are not installed in this area. In this regard, this territory is not identified by GNSS and linear-angular measurement data.

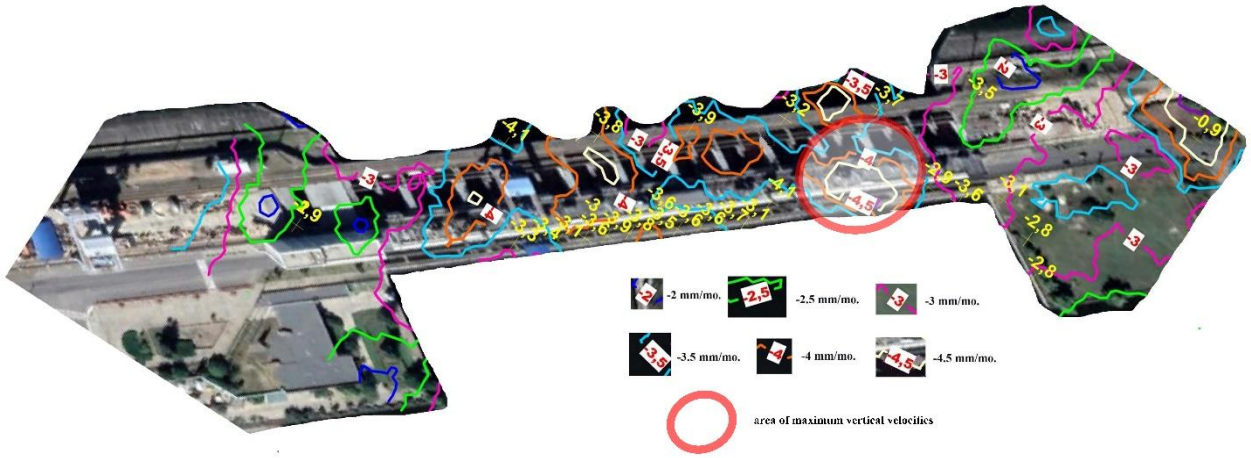

Fig. 12 Map of isolines of rates of vertical deformations of the dam surface for the period (2020.6 – 2021.1)

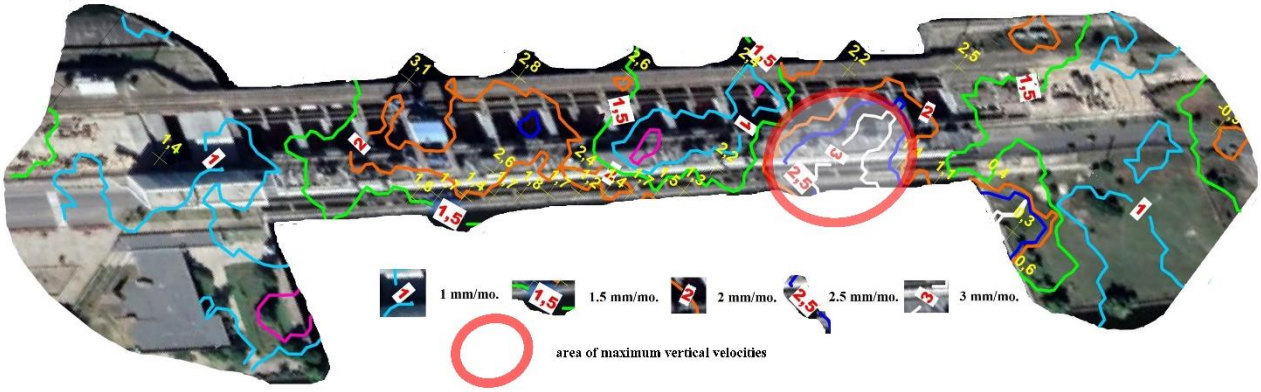

Fig. 13 Map of isolines of rates of vertical deformations of the dam surface for the period (2021.1 – 2021.6)

Conclusions

The research was conducted at the Kaniv hydroelectric power station using geodetic control points from the Stationary System for Monitoring the Spatial Displacement of Structures (SSMSDS). The SSMSDS was measured using GNSS and TPS, and all control point coordinates were determined with GEOMOS software. To compare the dam's surface vertical displacements, radar images were double-processed for a year, from August 2020 to August 2021, with a 12-day frequency. Both ground and satellite measurements showed similar temporal and spatial displacement patterns. The vertical displacement vectors of control points were opposite in direction for the first and second halves of each year. For the first half of the year, most items rose, while in the second half, they fell. This semiannual change led to the dam fluctuating up to 20mm annually, with the extremes occurring in February and August. Based on the data of radio interferometric measurements, the error in determining the vertical movement speeds of dam control points relative to the results obtained from GNSS and linear-angular measurements for the period of 2020.6-2021.1 is 0.41 mm/mo. The average speed during this period is -3.5 mm/mo. For the period of 2021.1-2021.6, the error is 0.85 mm/mo with an average speed of +1.7 mm/mo. By jointly processing radar images and GNSS and TPS data, the Kaniv HPP dam's vertical displacement velocities were spatially distributed, and anomalous velocity zones were identified. These zones can indicate hidden defects related to the dam's strength. This technology demonstrates the reliability of the results and the effectiveness of monitoring potentially dangerous objects like dams.

Declarations

Conflict of interest The authors declare no competing interests.

References

Africa I Flores-Anderson, Kelsey E Herndon, Rajesh Bahadur Thapa, Emil Cherrington (2019) The Synthetic Aperture Radar (SAR) Handbook: Comprehensive Methodologies for Forest Monitoring and Biomass Estimation. SERVIR Global Science Coordination Office, National Space Science and Technology Center. https://doi.org/10.25966/nr2c-s697

Aswathi J, Binoj Kumar RB, Oommen T, Bouali EH, Sajinkumar KS (2022) InSAR as a tool for monitoring hydropower projects: A review. Energy Geoscience 3 (2), 160–171. https://doi.org/10.1016/j.engeos.2021.12.007

Bernese GNSS Software. http://www.bernese.unibe.ch/

Bouali EH, Oommen T, Escobar-Wolf R (2017) Mapping of slow landslides on the Palos Verdes Peninsula using the California landslide inventory and persistent scatterer interferometry. Landslides 15 (9). https://doi.org/10.1007/s10346-017-0882-z

Cao Y, Li Z, Wei J, Hu J, Duan M and Feng G (2018) Stochastic modeling for time series InSAR: with emphasis on atmospheric effects. Journal of Geodesy 92 (2), 185–204. https://doi.org/10.1007/s00190-017-1055-5

Carlà T, Tofani V, Lombardi L, Raspini F, Bianchini S, Bertolo D, Thuegaz P, Casagli N (2019) Combination of GNSS, satellite InSAR, and GBInSAR remote sensing monitoring to improve the understanding of a large landslide in high alpine environment. Geomorphology 62–75. https://doi.org/10.1016/j.geomorph.2019.03.014

Chen CW, Zebker AH (2003) SNAPHU: statisticalcost, network-flow algorithm for phase unwrapping. Retrieved April 27, 2016.

Colesanti C, Wasowski J (2006) Investigating landslides with space-borne Synthetic Aperture Radar (SAR) interferometry. Engineering Geology 88 (3-4), 173-199. https://doi.org/10.1016/j.enggeo.2006.09.013

Copernicus Open Access Hub. https://scihub.copernicus.eu/

Crosetto M, Monserrat O, Cuevas M, Crippa B (2011) Spaceborne differential SAR interferometry: data analysis tools for deformation measurement. Rem. Sens. 3 (2), 305–318. https://doi.org/10.3390/rs3020305

Di Martire D, Iglesias R, Monells D, Centolanza G, Sica S, Ramondini M, Pagano L, Mallorquí JJ, Calcaterra D (2014) Comparison between differential SAR interferometry and ground measurements data in the displacement monitoring of the earth-dam of Conzadella Campania (Italy). Remote Sens. Environ. 148, 58–69.

Fárová K, Jelének J, Kopačková-Strnadová V, Kycl P (2019) Comparing DInSAR and PSI Techniques Employed to Sentinel-1 Data to Monitor Highway Stability: A Case Study of a Massive Dobkovičky Landslide, Czech Republic. Remote Sensing 11(22):2670. https://doi.org/10.3390/rs11222670

Ferretti A, Fumagalli A, Novali F, Prati C, Rocca F, Rucci A (2011) A New Algorithm for Processing Interferometric Data-Stacks: SqueeSAR. Transactions on Geoscience and Remote Sensing 49, 3460–3470.

Graham LC (1974) Synthetic interferometer radar for topographic mapping. Proc. IEEE, 62 (6), 763–768.

Heresh Fattahi, Falk Amelung (2014) InSAR uncertainty due to orbital errors. Geophysical Journal International 199 (1), 549–560. https://doi.org/10.1093/gji/ggu276

Herrera G, Gutiérrez F, García-Davalillo JC, Guerrero J, Notti D, Galve JP et al (2013) Multi-sensor advanced DInSAR monitoring of very slow landslides: The Tena Valley case study (central Spanish Pyrenees). Remote Sensing of Environment 128, 31–43. https://doi.org/10.1016/j.rse.2012.09.020

Honda K et al (2012) Application of exterior deformation monitoring of dams by DInSAR analysis using ALOS PALSAR. 2012 IEEE International Geoscience and Remote Sensing Symposium, 6649-6652, https://doi.org/10.1109/IGARSS.2012.6352074

Horb O, Nesterenko S, Afanasyev O & Baistruk O (2023) Directions of application of artificial intelligence in geodesic monitoring of buildings and structures. Municipal Economy of Cities 3 (177), 109-114. https://doi.org/10.33042/2522-1809-2023-3-177-109-114

Leica GeoMoS Monitoring Solution. https://leica-geosystems.com/products/total-stations/software/leica-geomos

Liu Y, Fan H, Wang L, Zhuang H (2021) Monitoring of surface deformation in a low coherence area using distributed scatterers InSAR: Case study in the Xiaolangdi Basin of the Yellow River, China. Bull. Eng. Geol. Environ. 80, 25–39. https://doi.org/10.1007/s10064-020-01929-1

Massonnet D & Feigl KL (1998) Radar interferometry and its application to changes in the Earth's surface. Reviews of geophysics 36(4), 441-500.

Meteopost: Archive of meteorological data. View the actual weather for a specific date. https://meteopost.com/weather/archive/

Nettis A, Massimi V, Nutricato R, Nitti DO, Samarelli S, Uva G (2023) Satellite-based interferometry for monitoring structural deformations of bridge portfolios. Automation in Construction 147, 104707. https://doi.org/10.1016/j.autcon.2022.104707

Pang Z, Jin Q, Fan P, Jiang W, Lv J, Zhang P, Cui X, Zhao C, Zhang Z (2023) Deformation Monitoring and Analysis of Reservoir Dams Based on SBAS-InSAR Technology−Banqiao Reservoir. Remote Sens. 15, 3062. https://doi.org/10.3390/rs15123062

Passah A, Sur SN, Abraham A, Kandar D (2023) Synthetic Aperture Radar image analysis based on deep learning: A review of a decade of research. Engineering Applications of Artificial Intelligence (IF 7.802). https://doi.org/10.1016/j.engappai.2023.106305

Pawluszek-Filipiak K, Borkowski A (2020) Integration of DInSAR and SBAS Techniques to Determine Mining-Related Deformations Using Sentinel-1 Data: The Case Study of Rydułtowy Mine in Poland. Remote Sensing 12(2):242. https://doi.org/10.3390/rs12020242

Perissin D (2016) Interferometric SAR multitemporal processing: techniques and applications. Multitemporal Remote Sensing. Springer, Cham, 20, 145–176. https://doi.org/10.1007/978-3-319-47037-5_8

Rosen PA, Hensley S, Joughin IR, Li FK, Madsen SN, Rodriguez E & Goldstein RM (2000) Synthetic aperture radar interferometry. Proceedings of the IEEE 88(3), 333-382.

SNAP. http://step.esa.int/downloads/6.0/installers/esa-snap_all_unix_6_0.sh

Tomás R, Cano M, García-Barba J, Vicente F, Herrera G, Lopez-Sanchez JM, Mallorquí JJ (2013) Monitoring an earthfill dam using differential SAR interferometry: La Pedrera dam, Alicante, Spain. Engineering Geology 157, 21-32. https://doi.org/10.1016/j.enggeo.2013.01.022

Tretyak K & Palianytsia B (2021) Research of seasonal deformations of the Dnipro HPP dam according to GNSS measurements. Geodynamics 1(30), 5-16. https://doi.org/10.23939/jgd2021.01.005

Tretyak K & Palianytsia B (2022) Research of the environmental temperature influence on the horizontal displacements of the Dnieper hydroelectric station dam (according to GNSS measurements). Reports on Geodesy and Geoinformatics 113 (1), 1-10. https://doi.org/10.2478/rgg-2022-0001

Tretyak K, Zayats O & Hrabovyi O (2023) Combined adjustment of GNSS observation results and slit meter measurements for the displacement detection at the Dniester HPP dam. Appl Geomat 15, 441–453. https://doi.org/10.1007/s12518-023-00502-1

Tretyak K & Palianytsia B (2023) Dam Spatial Temperature Deformations Model Development Based on GNSS Data. Journal of Performance of Constructed Facilities 37 (4). https://doi.org/10.1061/JPCFEV.CFENG-4312

Ullo SL, Addabbo P, Di Martire D, Sica S, Fiscante N, Cicala L, Angelino CV (2019) Application of DInSAR technique to high coherence Sentinel-1 images for dam monitoring and result validation through in situ measurements. IEEE J. Sel. Top. Appl. Earth Obs. Rem. Sens. 12 (3), 875-890. https://doi.org/10.1109/JSTARS.2019.2896989

Vajedian S, Motagh M, Nilfouroushan F (2015) StaMPS Improvement for Deformation Analysis in Mountainous Regions: Implications for the Damavand Volcano and Mosha Fault in Alborz. Remote Sens. 7, 8323-8347. https://doi.org/10.3390/rs70708323

Vázquez-Ontiveros JR, Ruiz-Armenteros AM, de Lacy MC, Gaxiola-Camacho JR, Anaya-Díaz M, Vázquez-Becerra GE (2023) Risk Evaluation of the Sanalona Earthfill Dam Located in Mexico Using Satellite Geodesy Monitoring and Numerical Modeling. Remote Sens. 15 (3), 819. https://doi.org/10.3390/rs15030819

Wang T, Perissin D, Rocca F et al (2011) Three Gorges Dam stability monitoring with time-series InSAR image analysis. Sci. China Earth Sci. 54, 720–732. https://doi.org/10.1007/s11430-010-4101-1

Xiao R, He X (2019) Deformation Monitoring of Reservoirs and Dams Using Time-Series InSAR. Geomatics and Information Science of Wuhan University 44 (9), 1334–1341. https://doi.org/10.13203/j.whugis20170327

Xiao R, Jiang M, Li Z, He X (2022) New insights into the 2020 Sardoba dam failure in Uzbekistan from Earth observation. International Journal of Applied Earth Observation and Geoinformation, 107, 102705. https://doi.org/10.1016/j.jag.2022.102705

Xiong X, Wang M, Gong C (2019) Study on Reservoir Earth Rock-Filled Dam Deformation Monitoring by MT-InSAR Technology. Journal of Geomatic, 78-81. https://doi.org/10.14188/j.2095-6045.2018167

Yagüe-Martínez N et al (2016) Interferometric processing of Sentinel-1 TOPS data. IEEE Transactions on Geoscience and Remote Sensing 54 (4), 2220-2234. https://doi.org/10.1109/TGRS.2015.2497902